Constrained sintering of alumina micro-ring films on stiff and compliant substrates: constriction or dilation?

Christine Jamin [b], Apurv Dash [a]*, Nachiketa Mishra [c], Rajendra K. Bordia [d], Olivier Guillon [a,b]

[a] Forschungszentrum Jülich GmbH, Institute of Energy and Climate Research: Materials Synthesis and Processing (IEK-1), D-52425, Jülich, Germany

[b] Institute of Materials Science, Technische Universität Darmstadt

Alarich-Weiss-Str. 2, D-64287, Darmstadt, Germany

[c] Department of Mathematics, Indian Institute of Information Technology, Design and Manufacturing, Kancheepuram, Chennai-600127, India

[d] Department of Materials Science and Engineering

Clemson University, Clemson, SC 29634 USA

*corresponding author. Tel.: +49 2461 61-9878; (Apurv Dash)

a.dash@fz-juelich.de

Email addresses:

Christine Jamin: ccjamin@gmx.de
Apurv Dash: a.dash@fz-juelich.de
Nachiketa Mishra: nmishra@iiitdm.ac.in
Rajendra K. Bordia: rbordia@clemson.edu
Olivier Guillon: o.guillon@fz-juelich.de

Keywords:

Thick film, patterned film, micro-molding in capillaries, constrained sintering, alumina

Abstract

The sintering behavior of ring-shaped alumina films on different types of substrates (polished sapphire and platinum coated sapphire) has been investigated. Variation of substrate material, layer thickness and heating schedule led to different interface properties which were quantified using the interfacial friction parameter as a measure of the slip distance of the free edge. This interfacial friction implies the compliance of the film-substrate interface, thus allowing the quantification of the ability of the free edges to slide along the substrate. Ring structures were made with outer radii of 100 - 500 μm and the ratios of inner to outer radii were 0.1 (broad ring segment with small inner hole) and 0.4 (narrow ring segment with big inner hole). During sintering, the outer film edge was found to recede in all systems, whereas the behavior of the free edge located at the inner hole was strongly dependent on the interfacial friction. When sintering of alumina micro-rings were carried out on sapphire substrate, a high interfacial friction resulted in the positive displacement of the inner edge, causing the inner hole to open. Sapphire substrates coated with platinum offered a lower interfacial friction resulting in the opening of the hole in a more distinct manner as compared to the uncoated sapphire substrates. As the thickness of the film also affects the interfacial friction, a thicker film (27 μm) on platinum coated substrate had very low friction. This resulted in a negative displacement of the inner ring leading to closing of the hole. These effects are in qualitative agreement with the predicted analytical model for constrained sintering of annular ceramic films. A combination of film thickness, substrate material and aspect ratio of the ring either leading to constriction or dilation of the annular alumina film were carefully investigated.

1. Introduction

The sintering of a continuous ceramic film on a dense substrate is a very precise example of constrained sintering. The coating of ceramic film is done by relatively easy processing techniques like tape casting, spin or dip coating. The sintering of films on fully dense substrates reported in the literature usually assume that all lateral strains are negligible and shrinkage is restricted to the out-of-plane direction [1],[2],[3],[4]. A limited number of theoretical and simulation studies have considered the possibility of non-zero lateral strains. These include analytical models [5],[6], finite-element simulations [7] or discrete element simulations [8],[9],[10].

As novel applications such as structural health monitoring [11] or micro ultrasonic transducers [12] require the printing of line structures for microns-sized strain gauges and heating elements with high precision without any post-processing defect, the prediction of lateral sintering strain is vital to near-net shaping. Similar stringent criteria are relevant to additive manufacturing of ceramics via selective laser sintering [13], since sequential sintering of individual stripe-shaped layers need to be bonded to the previously sintered layer without delamination or anisotropic shrinkage. Preliminary research has shown the possibility to fabricate a variety of geometries for the shape of the ceramic film deposited on a substrate by soft micro-molding techniques [14],[15].

In previous works [5],[6] interfacial sliding resistance was calculated by measuring the displacement of the straight film edge along the contact with the substrate in a continuous film during sintering. The sintering behavior of ring structures bonded to substrates with different friction parameters were predicted. Due to the experimental challenges described below, theoretical predictions could only be partially complimented by experimental data [16],[17],[18],[19],[20]. This is, in part, due to the fact that experimentalists face much higher quality requirements while exploring edge effects. Film edges must be well-formed and straight. In order to study edge effects in features with small size, the geometric fluctuations in edge width have to be much smaller than the total width. Typical fluctuations will be of the order of a few particle diameters. For investigating features in a few micron range, very fine particle size and specialized patterning techniques are required. Previous experimental research on the behavior of film edges during sintering was carried out with artificial film edges on continuous films generated by cutting, indenting or etching voids [16],[17],[20]. However, the film edges created by such destructive techniques are subjected to local damage or artifacts due to high energy etching techniques or mechanical machining, making accurate length measurements questionable. In some cases, the technique used to create the features modifies the densification behavior of the particles in the vicinity of the feature. Hence, in order to critically examine the predictions of the analytical model, specialized patterning techniques are needed which have recently become available and are used in this investigation.

In this paper, we report the experimental measurement of the interfacial sliding resistance for constrained sintering of annular alumina films, as a function of film thickness on two

different substrates (sapphire and Pt coated sapphire) using high-quality film edges. These edges were prepared by micro-molding in capillaries (MIMIC) [21], a patterning method that involves soft elastomer stamps that can be removed from the deposited film with virtually no damage to the stripe edges and very precise geometry. In addition, the constrained sintering behavior of ring-shaped features were measured and compared to the predictions of the Jagota and Hui model using the measured interfacial friction. To our knowledge, such an investigation has not been previously reported.

2. Description of Jagota and Hui model

Jagota and Hui [5],[6] have provided a description of the film-substrate interface of sintering films and its influence on lateral shrinkage and crack propagation. In their model, the three-dimensional governing equations of viscous materials [22] are reduced to a two-dimensional form by averaging stresses and velocities across the thickness. The boundary conditions are set based on the assumption that the shear stress τ along the interface is proportional to the in-plane shrinkage velocity v_i via a proportionality factor m which is a function of the film-substrate interfacial bonding and film thickness:

$$\tau = -m^2 v_i \tag{1}$$

Normalization of the governing equations by the defect size in the film leads to the interface friction parameter k:

$$k \equiv \frac{m^2(1-(\nu^P)^2)}{E^P} \tag{2}$$

k represents the inverse of the slip distance of the free edge in a sintering film. ν^P and E^P represent the viscous Poisson's ratio and the uniaxial viscosity respectively. An experimentally accessible expression for k is given by Bordia and Jagota [16]:

$$k = \frac{-\varepsilon_{free}(1+\nu^P)}{\Delta y} \quad (3)$$

Where Δy is the slip distance of the edge of a constrained film during sintering and ε_{free} represents the sintering strain of an identical free film sintered under the same conditions as the constrained film. This expression is valid for small changes in m and ν^P during densification. Small values of k correspond to large slip distances and thus indicate poor bonding, whereas large values of k correspond to well bonded interfaces and smaller slip distances. In addition, due to averaging of the interfacial traction across the film thickness, k should decrease as film thickness increases. This approach has been used to predict the conditions for crack growth in constrained sintering films which has been experimentally validated [16],[17]. It should be noted from Equation (3) that k has dimensions of inverse length (μm^{-1}). A good normalization for it is the film thickness or some other relevant feature size.

Experimental values for the interfacial friction parameters are not available in the literature. However, a normalized friction parameter has been calculated as the inverse slip distance for alumina [16] on smooth sapphire substrates as well as on platinum coated sapphire substrates. A summary is given in Table 1.

Table 1: Normalized friction parameter for different film/substrate material systems.

Film material	Substrate material	Thickness t [μm]	$k_{norm} = \frac{-1}{\Delta y}$ [μm^{-1}]	Interface type	Reference
Alumina	Sapphire	11.8	0.091	Stiff $k \propto \frac{1}{t}$	[16]
		24.7	0.053		
		42.5	0.024		
Alumina	Pt/Sapphire	11.8	0.018	compliant $k \propto \frac{1}{t^{1/2}}$	
		24.7	0.015		
		42.5	0.012		

From this limited data set, it can be seen that regardless of the film material, as expected, ceramic films on sapphire substrates exhibit stronger bonding compared to Pt coated substrates. Films on polycrystalline alumina substrates exhibit higher friction than their smooth, single crystal counterparts, indicating a possible effect of surface roughness on film adhesion. The interface friction parameter also depends on film thickness. For well-bonded interfaces, k is inversely proportional to the film thickness t, whereas for weakly bonded interfaces, it scales inversely with $\sqrt{t}$.

The sintering behavior of annular films with inner radius a and outer radius b constrained by rigid substrates has been modeled in terms of the interfacial sliding resistance, k [6]. The ceramic film is treated as a viscous body due to the mathematical similarity of viscous and small-strain elastic deformations. The velocity across the thickness was averaged and assumed to be uniform for the sake of simplicity of analysis. The exact solution of the interfacial model for solving the radial velocities are based on modified Bessel's function of the first and second kind. The details of the mathematical formulation are mentioned

by Jagota et al.[5] Parameters such as the lateral shrinkage of the inner and outer diameters as well as tangential and radial stresses in the film are different for strongly and weakly bonded films. High values of k lead to a rapid increase of radial stress starting from the unstressed free edges until a plateau is reached. Small values of k result in a slow stress increase with a maximum in the center of the annulus. This maximum is lower than the plateau values for high k. The displacement of the inner and outer boundary of the ring is strongly dependent on the sliding resistance, k. The radial velocity of the inner edge and outer edge of the annular alumina ring during sintering is modelled as a function of the friction factor in Figure 1. A ratio of inner to outer radius of 0.1 and 0.4 is considered. In this Figure, k has been normalized by the inner radius of the ring and the velocity v_r has been normalized by the both the radius (*a* or *b*) and velocity of a free edge (*s*) in an unconstrained film. For very low values of friction, both the inner and the outer radius decrease and the decrease is the same as unconstrained shrinkage of the film. Interesting boundary displacement is observed as k increases. For all values of k, the outer radius becomes smaller although the displacement decreases as k increases. It asymptotically approaches zero displacement as k approaches infinity as expected since in a fully constrained film, the edge cannot move. The outward displacement of the inner radius decreases rapidly as k increases and at relatively low values of $ka < 0.14$ the inner radius shrinks. There is a peak in the expansion at modest values of $k = 0.44$. Further, increase in k leads to a decrease in the expansion of the inner radius. As expected, this expansion also asymptotically approaches zero as k approaches infinity. For the case with a radius ratio (a/b) of 0.4, the transition from the contraction to the expansion of the inner ring is more gradual with respect to the normalized friction factor. The inner radius has a

negative velocity below $k = 0.32$. The outer radius has a finite negative velocity which approaches the value of zero asymptotically at a very high *ka* value unlike the case of *a/b* = 0.1 where the outer radius velocity approaches zero quickly at high friction values ($ka \geq 2$). Moreover, the magnitude of the outer radius velocity for *a/b* = 0.4 at low and intermediate friction values is higher as compared to the system of *a/b* = 0.1, this may result in more prominent opening of the hole in intermediate friction values for the system of *a/b* = 0.4. This interesting behavior has not been experimentally validated and it is the primary focus of the present work.

3. Experimental procedure

Elastomer stamps were custom made for the micro-molding in capillaries process. To make the elastomeric molds, CAD design of the desired ring structures (Figure 2) was transferred to a shadow mask by electron beam lithography. Through this mask, photoresist-coated silicon wafers of different thicknesses were irradiated with X-rays. After development, wafers with the desired film structures were obtained. The latter steps have been carried out at the Institut für Mikrostrukturtechnik, Karlsruhe Institute of Technology, Germany. A soft elastomer stamp with a negative pattern of the wafer was obtained by casting of an elastomer-hardener mixture (Sylgard 184, Dow Corning, Germany) which was cured for 4h at 80 °C and subsequently peeled off.

The aqueous slurry used for film preparation was made of 50 vol. % alumina powder with an average particle size, d_{50} of 150 nm (TM-DAR, Taimei Chemicals, Japan) dispersed

in deionized water. Its pH was set to 10 by adding concentrated ammonium hydroxide. A dispersant (Dolapix CE 64, Zschimmer Schwarz, Germany) in the amount of 0.7 mg per m^2 of the surface area of the particles was added to the suspension. The slurry was continuously stirred and cooled in ice during the fabrication process and then deagglomerated for ten minutes in an ultrasonic disperser (UP 200S, Dr Hielscher GmbH, Teltow, Germany). The slurry was kept on a rolling mill for 24h prior to use. The high solid loading was chosen to minimize drying shrinkage and stresses that may lead to cracking around cavities in the green samples.

The substrates used were smooth sapphire (Ra < 0.5 nm) with or without a sputtered Platinum interlayer. For sintering investigation of stiff film-substrate interface, plain sapphire substrates were used. To study the sintering of ring structures on a compliant surface, a platinum interlayer was sputtered onto the polished surface of the sapphire substrates by using a cycle of 4 x 4 min at 40 mA (EMitech K950X, Quorum Technologies, Ontario, Canada). A 2h annealing step at 400 °C was added to relax the deposition stresses inside the layer and avoid cracking. The initial thickness of the Pt coatings was 0.3 +/- 0.02 µm. Sintering temperatures of 1250 °C could be withstood for up to 4h.

Prior to deposition, the substrates were soaked in NaOH for 2h, cleaned in isopropanol in an ultrasonic bath for 3 min, rinsed with acetone using a paper towel, rinsed in ethanol and blown dry with liquid nitrogen. The surface was inspected for residue under an optical microscope. Samples that underwent an unsuccessful deposition cycle were cleaned in the same fashion.

For film deposition, a micro-drop of the aqueous alumina slurry was deposited onto the substrate and patterned by placing the elastomer stamp on top and softly squeezing it to

ensure complete adhesion. For every sample, a new stamp was fabricated since used stamps retained ceramic grains that created defects which acted as crack initiation centers in subsequently deposited samples.

With the deposition process described above, ring-shaped patterns with a controlled thickness (between 2 to 20 μm) were fabricated. Using optical microscopy, a minimum of two rings per set of conditions (film thickness and film-substrate interface) were chosen for detailed analysis. The selected rings were inspected to have a defect free film edge, a well-formed inner hole and that there is no outflow of slurry into the inner hole facilitating a distinct observation of film and substrate contrast during microscopy.

Before sintering, the ring structures were detached from the channels connecting them to the slurry reservoir. This was carried out using a micromanipulator (Model S-926, Signatone, Gilroy, USA). Here, the cut was placed a few microns away from the ring in order to avoid damage to the ring. This procedure left a small amount of the connecting channels as later seen in Figure 5.

Sintering of the samples were carried out using a heating rate of 25 °C/min up to 1200 °C followed by 10 °C up to the holding temperature. For films on plain sapphire, the sintering hold temperatures of 1450 °C for 5min and 1350 °C for 4h were chosen. The continuous Pt coating on sapphire substrates was observed to break into islands at temperature more than 1400 °C. So for films on Pt coated substrates, the sintering temperatures were lowered to 1350 °C for 5min and 1250 °C for 4h. Prior research has shown that at 1350 °C, unconstrained samples made from the same powder with comparable starting densities around 55 % reach ca. 89 % of the theoretical density after a 5 min holding time [23] and isotropic strains around 4 % [24]. Since the ring segments have lateral

dimensions of d=(a-b)/2 with d ranging from 30 μm to 112.5 μm, a 4% lateral strain corresponds to an edge displacement value of 0.6 μm to 2.25 μm. After 4h at 1250 °C, densities reach 98 % with isotropic true sintering strains of -0.17. Due to these high free sintering strains and the presence of quasi-free densification near the stripe edges [25], non-negligible changes in width could be expected even in the presence of a constraining substrate, making measurements of lateral strain by SEM possible with the necessary accuracy.

Lateral dimensions of the rings were measured using top view scanning electron microscope (SEM) pictures. Displacement of the inner and outer ring edges was calculated as half the difference of the outer and inner diameter before and after sintering. Measurement lines were chosen normal to the disconnected channels in order to minimize the effect from the small amount of channel adherent to the ring.

The interface friction sliding resistance, k was calculated for every sintered film-substrate system using Equation (3). Here, v^P as a function of density for TM-DAR alumina was taken from Zuo et al. [26] who have validated Venkatachari's results [27] for the viscous Poisson coefficient. The free sintering strain of a bulk specimen with matching green density subjected to the same sintering cycle as the films was obtained from free sintering experiments on cylindrical samples. The displacement of the free edge, Δy, was calculated as half the difference in width of a 100 μm wide constrained stripe before and after sintering [25]. Height profiles were measured in the green and sintered state using white light interferometry (NV6200, ZygoLot GmbH, Darmstadt, Germany) for alumina stripes of similar heights and thicknesses made out of the same slurry and with the same procedure.[25,28] The uniformity of the film height of micro-rings were considered similar

to that of striped. Moreover, curvature in the stripes were only located in the edges (small area equivalent to the film thickness). As the radius of the micro ring is large compared to the thickness of the film, we have neglected the curvature effects in all cases.

4. Results and discussion

For comparing the experimental results of inner and outer edge displacement of alumina micro-rings with the analytical model, the friction factor needed to be calculated. The friction parameters were extracted by sintering simple alumina strips on stiff (sapphire) and compliant (Pt coated sapphire) substrates. In Figure 3 the measured constrained displacement of a straight edge (Δy) for 100 μm wide stripes is presented as function of film thickness and its square root. As the friction parameter also depends on the film thickness, a wide combination of strip thickness-substrate material was investigated for edge displacement to obtain every possible values of k. The calculated experimental interfacial sliding resistance, k (using Equation (3)) is shown as a function of the film thickness and its square root. Due to higher sintering temperatures (1350 °C on continuous Pt and 1450 °C on sapphire), displacement on sapphire substrate is slightly higher than on Pt/sapphire substrate. The data was analyzed using this approach since from prior studies (summarized in Table 1), k is inversely proportional to Δy for stiff interface and inversely proportional to the square root of Δy for compliant substrates. The nature of the plot of k is equivalent to y = 1/x in both the cases, whereas the nature of plot of Δy is equivalent to y = x, confirming the previous studies. Sintering of alumina stripes exhibit a linear increase of the upper edge displacement, as expected for stiff interfaces and strongly bonded films. In case of platinum coated sapphire, the same phenomena

are observed with the distinction that here, the upper edge displacement scales with the square root of the film thickness consistent with the behavior of a compliant interface. Here, too, the regular friction parameter decreases according to Equation (3) and reaches a plateau after a certain thickness. Thus, a threshold thickness-to-width ratio seems to exist that limits the applicability of Jagota's model to real film systems.

In all studied rings, shrinkage of the outer ring radius *b* is observed during sintering. A negative edge displacement is found for all interfaces, its extent being dependent on interface stiffness as observed in case of the stripes. The behavior of the inner ring radius *a* is found to depend on film thickness, as thick films experience hole closure, while the outer ring shrinks. The inner hole in thin films, however, grows. A closer look on the interface properties reveals a correlation between hole opening or closure and the product of the friction parameter times the inner hole radius, as shown in Figure 4. For the system with a ring aspect ratio of 0.1 and 0.4 there is qualitative agreement of our observations with Jagota's prediction as shown in Figure 1. [5]

The trend in the velocity of the free edges as predicted by Jagota resembles the trend of ΔD in our experiments. Firstly, the outer free edge of the ring shrinks throughout the entire range of ka, but to a lesser degree with increasing friction factor. Secondly, the displacement of the inner free edge is negative for very compliant interfaces, resulting in closure of the hole by the inward pressure of the retreating outer free edges. At intermediate values, starting at $ka = 1.0$, hole opening occurs and quickly reaches a maximum value before attaining a plateau at $ka = 1.4$ as shown in Figure 4(a). This indicates that the extent of hole opening is less in the case of very stiff interfaces as

compared to intermediate stiffness with $0.5 < ka \leq 1.5$ in the case of the radius ratio of 0.1.

The same trend is observed for the rings with a radius ratio of 0.4 (Figure 4(b)). Here, the transition from negative to positive displacement is even more pronounced. In both systems, the plateau value of the inner edge displacement is between 3 μm and 4 μm, whereas the displacement of the outer edge reaches 10 μm. The outer edge displacement curves are similar for both systems, whereas the inner edge displacement curve starts from a significantly lower value in case of the 0.4 system. The latter, narrower ring thus experiences stronger closure of the hole for very low friction of the interface ($ka < 3.7$) The difference in the extent of hole opening for intermediate and higher stiffness is very moderate for radius ratio of 0.4. This is also in agreement with the analytical model developed by Jagota et al. as shown in Figure 1(b). [5]

Figure 5 shows the scanning electron micrographs depicting the green as-fabricated alumina micro-rings and the corresponding sintered microstructures on Pt coated sapphire and pure sapphire substrate. Horizontal yellow lines are added as a guide for the readers to realize the extent of hole opening during sintering for various substrates. The differences in the hole diameter are very subtle as lie in the micron range. Careful investigations yielded reproducible results with standard deviation which is always mentioned in the data representation in Figure 3 and 4. Rings with different radius ratio of 0.1 and 0.4 are shown in (a) and (d) respectively. The rings sintered on Pt/sapphire substrate (b,e) have opened more than the rings sintered on sapphire substrate (c,f).

Furthermore, random radial cracking was observed in the inner hole in some ring configurations. Examples of inner holes with radius ratio of 0.1 and outer diameter of 50 µm for low, intermediate and high ka are shown in Figure 6. Cracking is not observed in the system that undergoes hole closure at the lowest value of ka. In the intermediate range, however, severe random radial cracking similar to the crack pattern observed in small round cavities in wide stripes is observed. At the highest values of ka, cracking also occurs, but to a lesser degree than in the intermediate range. At the outer ring, cracking does not occur at all. These observations are consistent with Jagota's predictions on the evolution of tangential stresses throughout the ka range. As in case of the round cavities in wide stripes, holes with a high diameter do not undergo cracking. For instance, in the system with a radius ratio of 0.4 and an outer diameter of 100 µm, cracking was never observed.

The behavior of ring structures during sintering was found to be consistent with the prediction made by Jagota et al. [5]. Several aspects were confirmed: Firstly, a transition from hole closure in low friction systems to hole opening in intermediate friction systems was observed both in narrow rings with a radius ratio of 0.4 system and wide rings with a radius ratio of 0.1. The shape of the displacement curves obtained in this work is in good agreement with the normalized radial velocity of the outer and inner free edges predicted in the model.

Hole closure was stronger in the narrow ring. This is supposed to be caused by the interference of the lateral stress fields that originate from both edges similar to the effects observed in narrow stripes. A section through a ring of outer diameter 100 µm and inner

diameter 40 µm with a film thickness of 27 µm is comparable to a 30 µm wide stripe whose cross section is entirely made up of two overlapping edge zones. Thus, narrow ring systems show quasi-free sintering behavior with non-zero lateral strains throughout their entire cross section. This is consistent with the distribution of radial stresses over the ring cross section shown in [6]. Stresses at the outer and inner free surface are zero and rise quickly in high friction systems ($ka \geq 2$ for $\frac{a}{b} = 0.1, ka \geq 12$ for $\frac{a}{b} = 0.4$) to a constant interior value. This matches the behavior of wide stripes with their separation in constrained mid-section and freely shrinking edge zones, as presented in the stress distributions modelled by finite element method [7]. The fact that the plateau values of the inner and outer edge displacement are similar in narrow and wide stripes leads to the assumption that as soon as there is no more interference between outer and inner edge, the edge zones are equivalent and merely separated by an increasingly large mid-section resulting in the dilation of the hole. Again, this is consistent with the behavior observed in sintering stripes.

Jagota's prediction on tangential hoop stress distribution is also confirmed qualitatively by the present experiments. According to the model, tangential stresses are maximal at the inner free surface and partially relaxed at the outer ring surface. The absolute value of the maximum stress scales with ka. In our experiments, evidence for high tangential stresses at the inner ring was found in the high ka systems in the form of radial cracking (shown in Figure 6). Stresses at the outer and inner free surface are zero and rise quickly in high friction systems (*ka* ≥ 2) to a constant interior value in the middle of the ring (intermediate values of *r/a* (as shown in Figure 7). The fact that the plateau values of the inner and outer edge displacement are similar in narrow and wide stripes leads to the

assumption that as soon as there is no more interference between outer and inner edge, the edge zones are equivalent and merely separated by an increasingly large mid-section. In the system with the lowest friction, no such cracks were formed.

The effect of the substrate material on the friction parameter is consistent with the differing degree of constraint observed in the stripes. The lowest friction was observed in the thickest system (27 μm) followed by the 8 μm rings on platinum coated sapphire. The highest friction was found in 8 μm rings on sapphire.

5. Conclusion

By using micro-molding-in-capillaries technique, alumina films of micro-ring geometry (outer diameter: 100/200 μm, inner diameter: 10/20/40/80 μm) were deposited and sintered on platinum coated sapphire and pure sapphire offering compliant and stiff interfaces respectively. Inner to outer radius ratios of 0.1 and 0.4 and film thickness of 8 and 27 μm were investigated. The displacement of the free edge of the outer and inner radius was studied to understand the effect of substrate on the sintering and shape change of the rings. The friction parameter values were extracted by studying the displacement of the free edge by sintering films of alumina stripes (100 μm wide) and were applied to the sintering of micro-rings. The constriction or dilation of the micro-ring during sintering was decided by the interfacial friction between the alumina film and the substrate. The thickness of the film affects the resistance offered to the relative mass diffusion with respect to the substrate. A wide combination of substrate-film thickness-radius ratio-outer diameter was investigated for assessing the interfacial friction factor. A friction dependent transition of hole closure to hole opening was found that is in very good

agreement with model predictions. A higher thickness of the film (27 μm) on Pt/sapphire substrate offers the least interfacial friction and results in the hole closure of the micro-ring. The hole closure was very vivid for the micro-ring with radius ratio 0.4. Intermediate interfacial friction was obtained by a lower film thickness (8 μm) on Pt/sapphire substrate, this resulted in the opening of the hole in a clear manner for a radius ratio of 0.1 and not so striking for a radius ratio of 0.4. Further increase in interfacial friction was obtained by the use of pure sapphire substrate. Higher interfacial friction resulted in the opening of the hole in both the case of radius ratio of 0.1 and 0.4 but the extent of dilation is lower as compared to intermediate friction values.

6. References

[1] R.K. Bordia, G.W. Scherer, On Constrained Sintering - I. Constitutive Model for a Sintering Body, Acta Metall. 36 (1988) 2393–2397. https://doi.org/10.1016/0001-6160(88)90189-7.

[2] R.K. Bordia, G.W. Scherer, On Constrained Sintering - II. Comparison of Constitutive Models, Acta Metall. 36 (1988) 2399–2409. https://doi.org/10.1016/0001-6160(88)90190-3.

[3] R.K. Bordia, R. Raj, Sintering Behavior of Ceramic Films Constrained by a Rigid Substrate, J. Am. Ceram. Soc. 68 (1985) 287–292. https://doi.org/10.1111/j.1151-2916.1985.tb15227.x.

[4] D.J. Green, O. Guillon, J. Rödel, Constrained sintering: A delicate balance of scales, J. Eur. Ceram. Soc. 28 (2008) 1451–1466. https://doi.org/10.1016/j.jeurceramsoc.2007.12.012.

[5] A. Jagota, C.Y. Hui, Mechanics of sintering thin films - I. Formulation and analytical results, Mech. Mater. 9 (1990) 107–119. https://doi.org/10.1016/0167-

6636(90)90034-D.

[6] A. Jagota, C.Y. Hui, Mechanics of sintering thin films - II. Cracking due to self-stress, Mech. Mater. 11 (1991) 221–234. https://doi.org/10.1016/0167-6636(91)90004-J.

[7] Y. Zhao, L.R. Dharani, Theoretical model for the analysis of a ceramic thin film sintering on a non-sintering substrate, Thin Solid Films. 245 (1994) 109–114. https://doi.org/10.1016/0040-6090(94)90885-0.

[8] C.L. Martin, R.K. Bordia, The effect of a substrate on the sintering of constrained films, Acta Mater. 57 (2009) 549–558. https://doi.org/10.1016/j.actamat.2008.09.041.

[9] C.L. Martin, Z. Yan, D. Jauffres, D. Bouvard, R.K. Bordia, Sintered ceramics with controlled microstructures: Numerical investigations with the Discrete Element Method, J. Ceram. Soc. Japan. 124 (2016) 340–345. https://doi.org/10.2109/jcersj2.15269.

[10] A. Hashibon, R. Schubert, T. Breinlinger, T. Kraft, A DEM contact model for history-dependent powder flows, Comput. Part. Mech. 3 (2016) 437–448. https://doi.org/10.1007/s40571-015-0099-7.

[11] I. Wirth, Sensor Technology, (2012). https://www.ifam.fraunhofer.de/en/Profile/Locations/Bremen/Shaping_Functional_Materials/Functional_Printing/Sensor_Technology.html (accessed April 2, 2021).

[12] D. Wang, E. Filoux, F. Levassort, M. Lethiecq, S.A. Rocks, R.A. Dorey, Fabrication and characterization of annular-array, high-frequency, ultrasonic transducers based on PZT thick film, Sensors Actuators A Phys. 216 (2014) 207–213. https://doi.org/10.1016/j.sna.2014.05.026.

[13] J.P. Deckers, K. Shahzad, L. Cardon, M. Rombouts, J. Vleugels, J.-P. Kruth, Shaping ceramics through indirect selective laser sintering, Rapid Prototyp. J. 22 (2016) 544–558. https://doi.org/10.1108/RPJ-10-2014-0143.

[14] S. Seils, R. Baraki, C. Jamin, O. Guillon, Free-standing patterned ceramic structures obtained by soft micromolding, Adv. Eng. Mater. 13 (2011) 502–508.

https://doi.org/10.1002/adem.201100013.

[15] J.E. ten Elshof, S.U. Khan, O.F. Göbel, Micrometer and nanometer-scale parallel patterning of ceramic and organic-inorganic hybrid materials, J. Eur. Ceram. Soc. 30 (2010) 1555–1577. https://doi.org/10.1016/j.jeurceramsoc.2010.01.016.

[16] R.K. Bordia, A. Jagota, Crack Growth and Damage in Constrained Sintering Films, J. Am. Ceram. Soc. 76 (1993) 2475–2485. https://doi.org/10.1111/j.1151-2916.1993.tb03969.x.

[17] D. Frame, Microstructure Development and Crack Growth in Constrained Electrolytes, University of Washington, 2006.

[18] X. Wang, A. Atkinson, Microstructure evolution in thin zirconia films: Experimental observation and modelling, Acta Mater. 59 (2011) 2514–2525. https://doi.org/10.1016/j.actamat.2010.12.056.

[19] X. Wang, J.-S. Kim, A. Atkinson, Constrained sintering of 8mol% Y2O3 stabilised zirconia films, J. Eur. Ceram. Soc. 32 (2012) 4121–4128. https://doi.org/10.1016/j.jeurceramsoc.2012.05.036.

[20] X. Wang, Z. Chen, A. Atkinson, Crack formation in ceramic films used in solid oxide fuel cells, J. Eur. Ceram. Soc. 33 (2013) 2539–2547. https://doi.org/10.1016/j.jeurceramsoc.2013.04.032.

[21] E. Kim, Y. Xia, G.m, Whitesides: Micromolding in capillaries: Applications in materials science, J. Am. Chem. Soc. 1185722 (1996) 5722–5731.

[22] G.W. Scherer, T. Garino, Viscous Sintering on a Rigid Substrate, J. Am. Ceram. Soc. 68 (1985) 216–220. https://doi.org/10.1111/j.1151-2916.1985.tb15300.x.

[23] T. Rasp, C. Jamin, A. Wonisch, T. Kraft, O. Guillon, Shape distortion and delamination during constrained sintering of ceramic stripes: Discrete element simulations and experiments, J. Am. Ceram. Soc. 95 (2012) 586–592. https://doi.org/10.1111/j.1551-2916.2011.04939.x.

[24] O. Guillon, S. Krauß, J. Rödel, Influence of thickness on the constrained sintering of alumina films, J. Eur. Ceram. Soc. 27 (2007) 2623–2627.

https://doi.org/10.1016/j.jeurceramsoc.2006.10.007.

[25] C. Jamin, T. Rasp, T. Kraft, O. Guillon, Constrained sintering of alumina stripe patterns on rigid substrates: Effect of stripe geometry, J. Eur. Ceram. Soc. 33 (2013) 3221–3230. https://doi.org/10.1016/j.jeurceramsoc.2013.06.016.

[26] R. Zuo, E. Aulbach, J. Rödel, Viscous Poisson's ratio coefficient determined by discontinuous hot forging, J. Mater. Res. 18 (2003) 2170–2176. https://doi.org/10.1557/JMR.2003.0303.

[27] K.R. Venkatachari, R. Raj, Shear Deformation and Densification of Powder Compacts, J. Am. Ceram. Soc. 69 (1986) 499–506. https://doi.org/10.1111/j.1151-2916.1986.tb07452.x.

[28] C. Jamin, T. Rasp, T. Kraft, O. Guillon, Constrained Sintering of Alumina Stripes on Rigid Substrates: Effect of Substrate Roughness and Coating, J. Am. Ceram. Soc. 98 (2015) 3988–3995. https://doi.org/10.1111/jace.13799.

Figures:

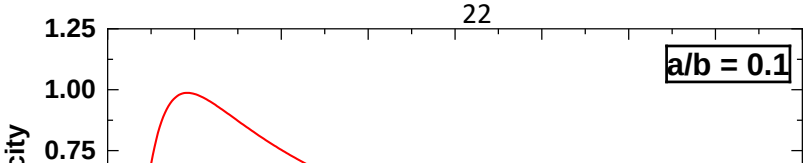

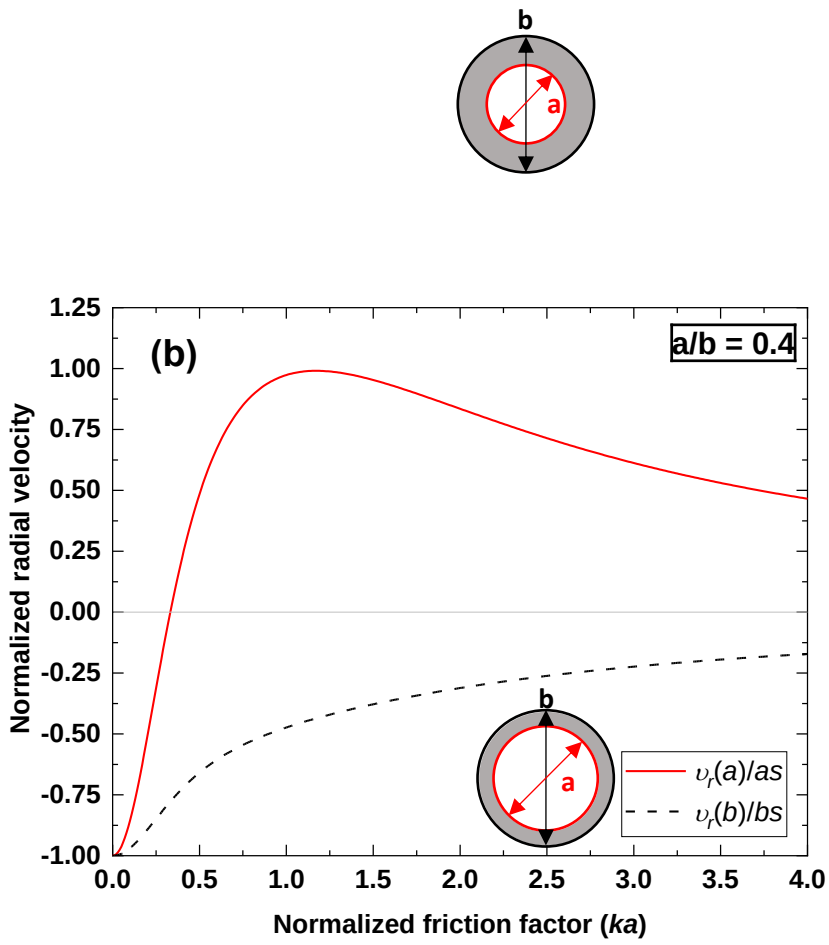

Figure 1: Normalized radial velocity for the outer and inner free edge of an annular ceramic film as a function of normalized interfacial friction factor. (a) shows the case with an inner to outer radius ratio of 0.1 and (b) shows the case with a radius ratio of 0.4 as used in the present study (a/b=0.1;0.4), Adapted from [5].

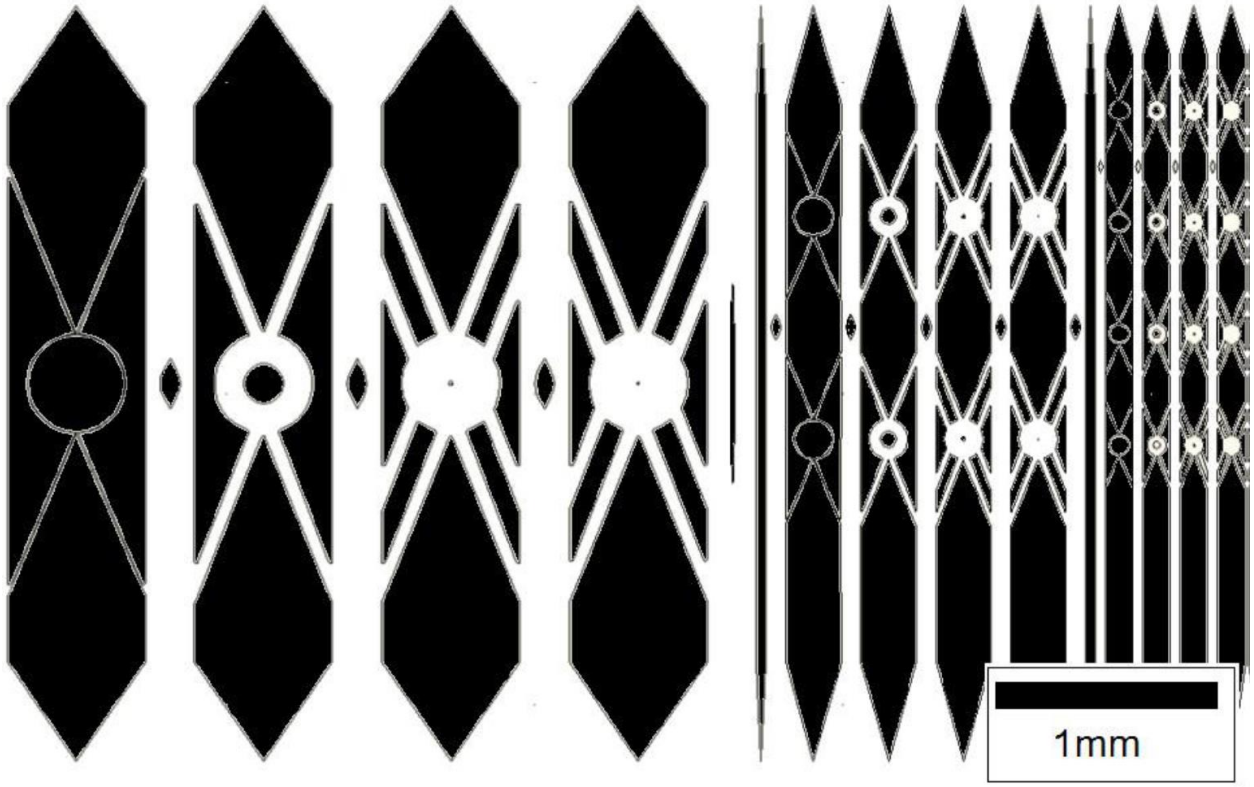

Figure 2: CAD pattern of ring structures connected to the slurry reservoir by beams oriented 45° with respect to the slurry channels. Areas covered by ceramic film material (slurry channels and rings) are represented in white, uncoated substrate is represented in black.

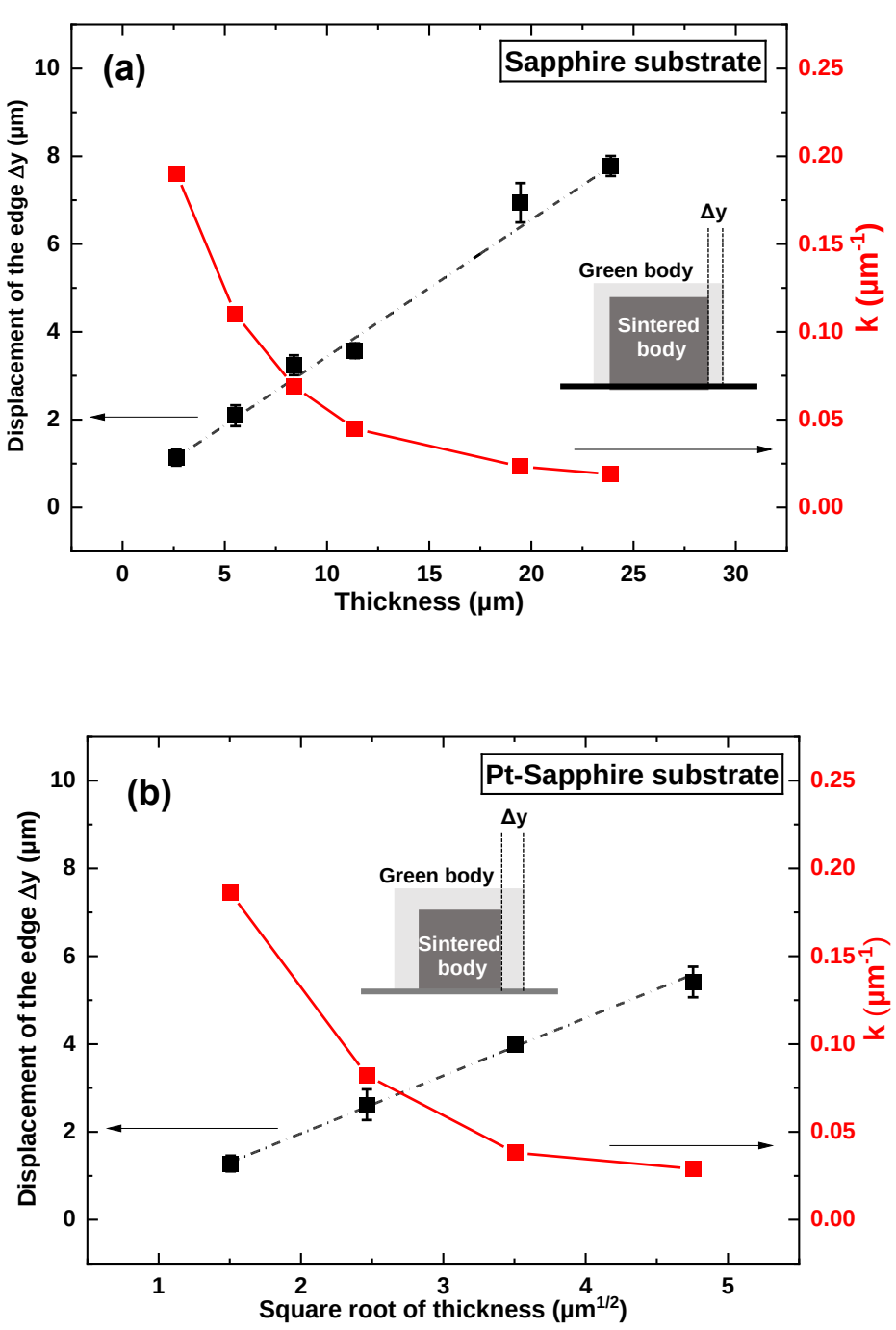

Figure 3: Edge displacement and friction parameter for 100 μm wide alumina stripes on different substrates with respect to the thickness of the film (a) Sapphire substrate (stiff interfaces), (b) Pt coated sapphire substrate (compliant interfaces).

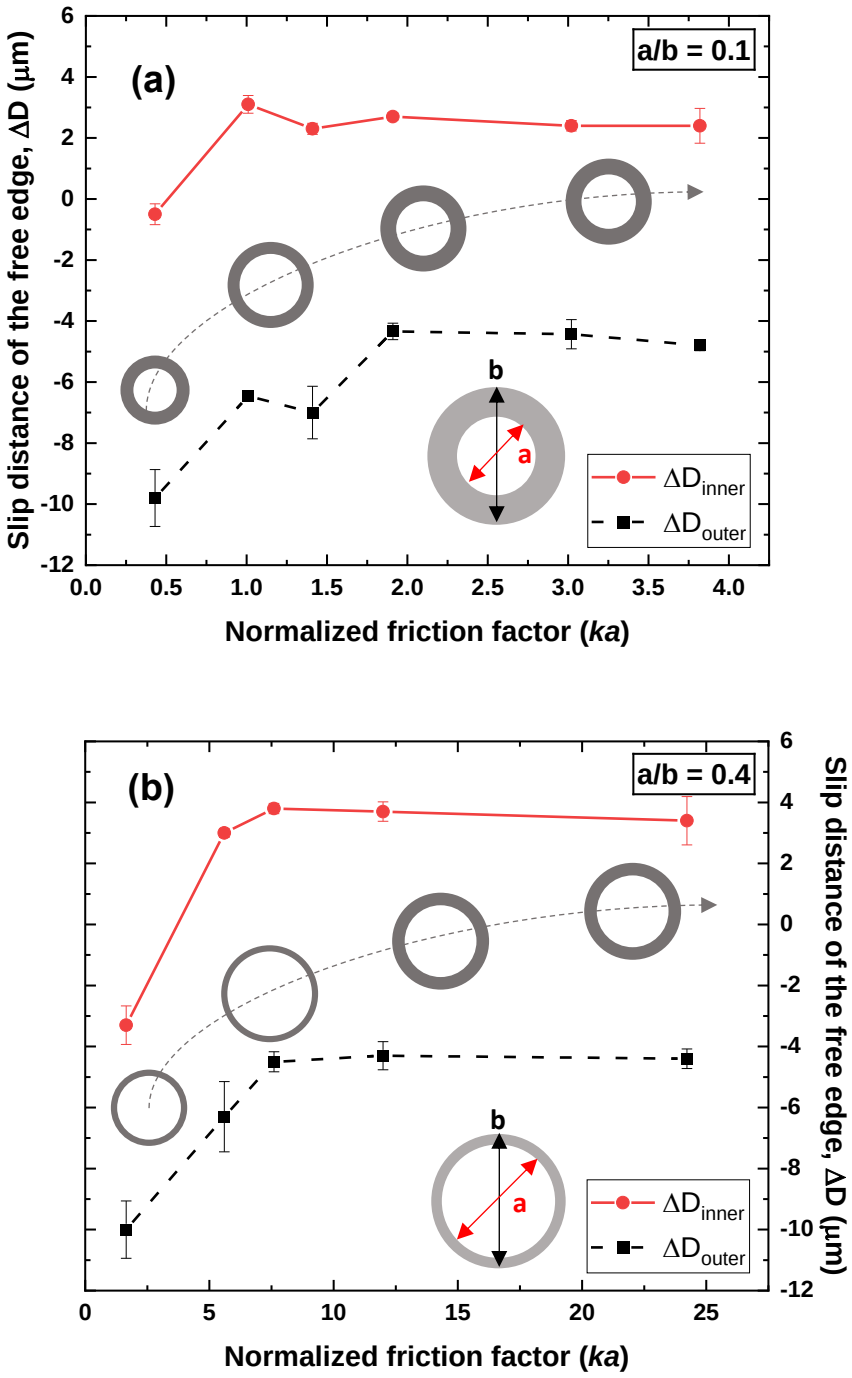

Figure 4: Slip distance of the inner and outer free edges as a function of the product of friction parameter and inner radius in ring systems with radius ratio of 0.1 (a) and 0.4 (b). The inset shows the evolution of the dimensions of the sintered ring, please note that the rings shown are only for representation and do not correspond to the actual scale.

Figure 5: Scanning electron micrographs of green and sintered alumina micro rings, (a,b,c) alumina ring with a/b = 0.1, (a) as-micromolded, (b) sintered ring on Pt/sapphire substrate, (c) sintered ring on sapphire substrate, (d,e,f) alumina ring with a/b = 0.4, (d) as-micromolded, (e) sintered ring on Pt/sapphire substrate, (f) sintered ring on sapphire substrate. All the rings had an outer diameter of 100 µm. The horizontal yellow lines are a guide for the readers to see the opening of the holes.

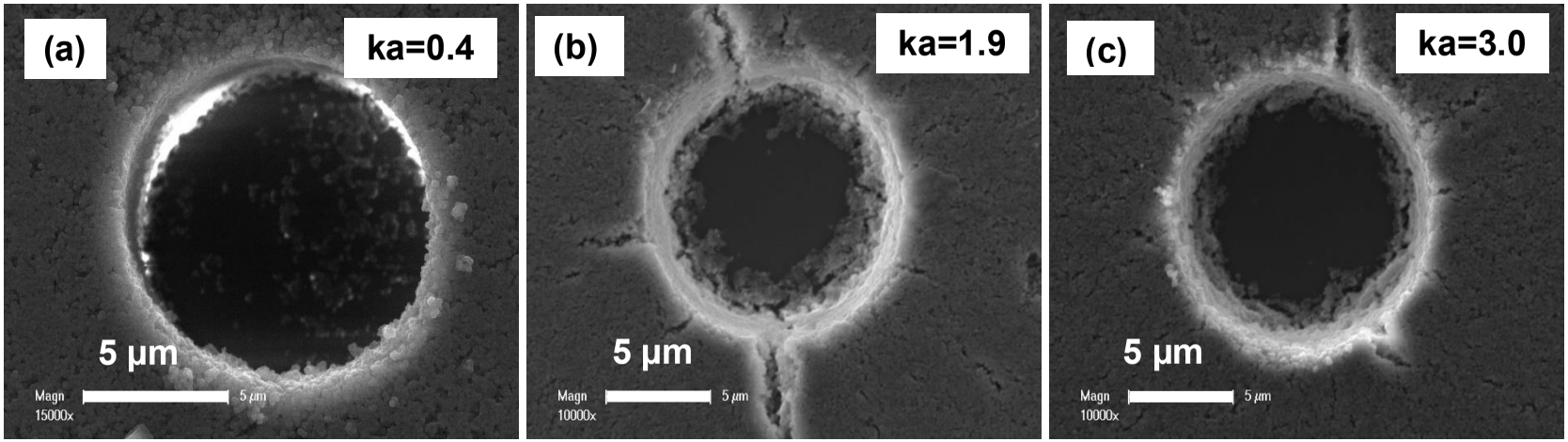

Figure 6: Micrographs of cracks formed at the inner ring in the 0.1 system on plain sapphire with a film thickness of (a) 27 µm, (b) 8 µm on Pt/Sapphire substrate, (c) 8 µm.

1

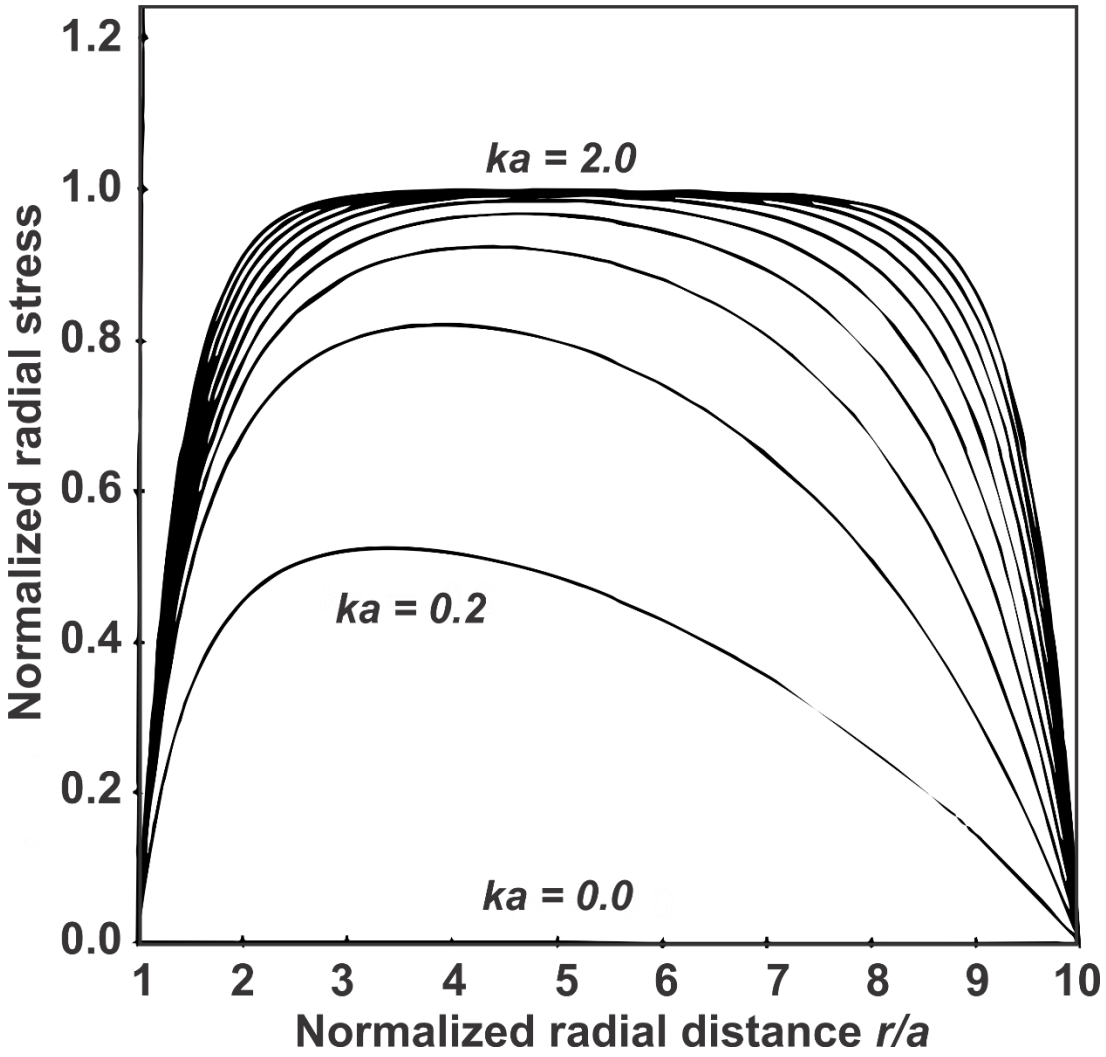

Figure 7: Normalized radial stress as a function of normalized radial distance. Adapted from [5]. This is complimentary to the radial cracks shown in Figure 6.